ACS OMEGA

Open Access

http://pubs.acs.org/journal/acsodf

Article

Neolignans and Diarylnonanoid Derivatives with Anti-inflammatory Activity from *Myristica fragrans* Houtt. Seeds

Tam Thi Le, Jonghwan Kim, Tae Kyeom Kang, Wook-Bin Lee, Myungsuk Kim, Chung Sub Kim,* and Sang Hoon Jung*

Cite This: *ACS Omega* 2024, 9, 35170−35181

Read Online

ACCESS | Metrics & More | Article Recommendations | Supporting Information

ABSTRACT: *Myristica fragrans* Houtt. is rich in lignans, neolignans, and diarylnonanoids, with well-documented anti-inflammatory properties. However, there is limited research on the conjugated forms of diarylnonanoids, neolignans, monoterpenes, and others and their anti-inflammatory effects. Our study isolated 33 new compounds (**2**−**7**, **9**−**22**, and **41**−**52**), including two neolignans, alongside various neolignan-diarylnonanoid, propenylbenzene-diarylnonanoid, 2,3-dimethylbutane-type lignan-diarylnonanoid, and monoterpene-diarylnonanoid conjugates, along with previously reported compounds (**1**, **8**, and **23**−**40**). Their chemical structures were determined via spectroscopic analyses. Compounds **2**, **4**, **9**, **11**, **12**, **14**, **17**, and **18** exhibited potent inhibition of NF-κB/AP1 and IRF signaling induced by TLR agonists. Notably, stereoisomers showed distinct behavior, while 10*R*,11*R*-isomers induced cytotoxicity, and 10*S*,11*R*-isomers produced contrasting effects, especially within group-I compounds.

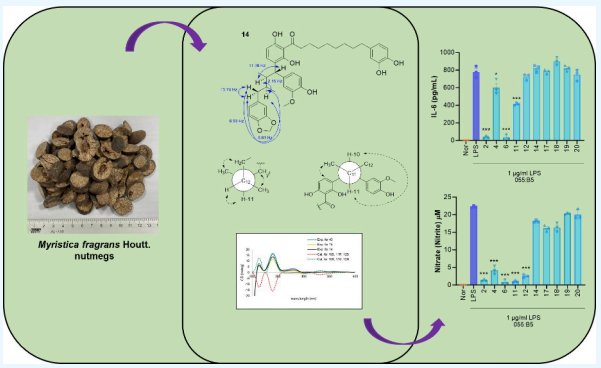

INTRODUCTION

The nutmeg tree, scientifically named *M. fragrans*, is an evergreen tropical plant renowned for its delightful fragrance and flavor. It is extensively cultivated for economic purposes in several Southeast Asian nations such as Indonesia and Thailand, as well as in East Asian countries like Japan and China, and also in South Africa and India.[1] The *M. fragrans* plant has three major commercial products: mace, nutmeg, and essential oils, which are widely used as spices in food products.[2] Various parts of the plant have been used in traditional medicine, such as *M. fragrans* mace in traditional Chinese medicine for stomach ailments and as a possible abortifacient.[3] In Ayurvedic medicine, mace is used to treat asthma and gastrointestinal complaints.[4] Nutmeg has a long history of medicinal use for treating conditions such as diarrhea, rheumatism, headaches, and stimulating appetite. Nutmeg oil is utilized for treating rheumatism, intestinal disorders, and kidney-related issues due to its antiseptic and analgesic properties.[1]

M. fragrans contains a wide range of botanical compounds, such as lignans, neolignans, diphenylalkanes, phenylpropanoids, terpenoids, alkanes, fatty acids, and fatty acid esters, as well as some minor constituents like steroids, saponins, triterpenoids, and flavonoids.[5−9] These compounds are present in various plant parts, such as the aril (mace), nutmeg (seed), stem bark, and fruit pericarp, and have been reported to have pharmacological effects such as anti-infammatory and analgesic activities,[10,11] antioxidant activities,[8] antibacterial and anti-fungal activities,[12] and anticancer and chemopreventive activities,[13] suggesting the potential medicinal value of *M. fragrans*.

Diarylnonanoids, lignans, and neolignans are key metabolites identified from *M. fragrans*, and their anti-inflammatory activities have been documented.[14−18] However, there is limited information about the conjugated forms of diarylnonanoids, neolignans, monoterpenes, and other compounds as well as their anti-inflammatory properties. In this study, a diverse array of neolignan-diarylnonanoid, 2,3-dimethylbutane-type lignan-diarylnonanoid, propenylbenzene-diarylnonanoid, and rare monoterpene-diarylnonanoid conjugates were isolated from the seeds of *M. fragrans*. Some of these compounds were investigated for their impact on NF-κB/AP1 and IRF activity as well as their role in regulating the production of proinflammatory cytokines and nitric oxide.

RESULTS AND DISCUSSION

Utilizing repeated column chromatography on the 75% EtOH extract obtained from *M. fragrans* nutmegs, we have identified and isolated one new dihydrobenzofuran neolignan (**20**), one

Received: June 17, 2024
Revised: July 19, 2024
Accepted: July 22, 2024
Published: July 30, 2024

https://doi.org/10.1021/acsomega.4c05649
ACS Omega 2024, 9, 35170−35181

Chart 1. Structures of Isolated Compounds 1- 22 and 41- 52

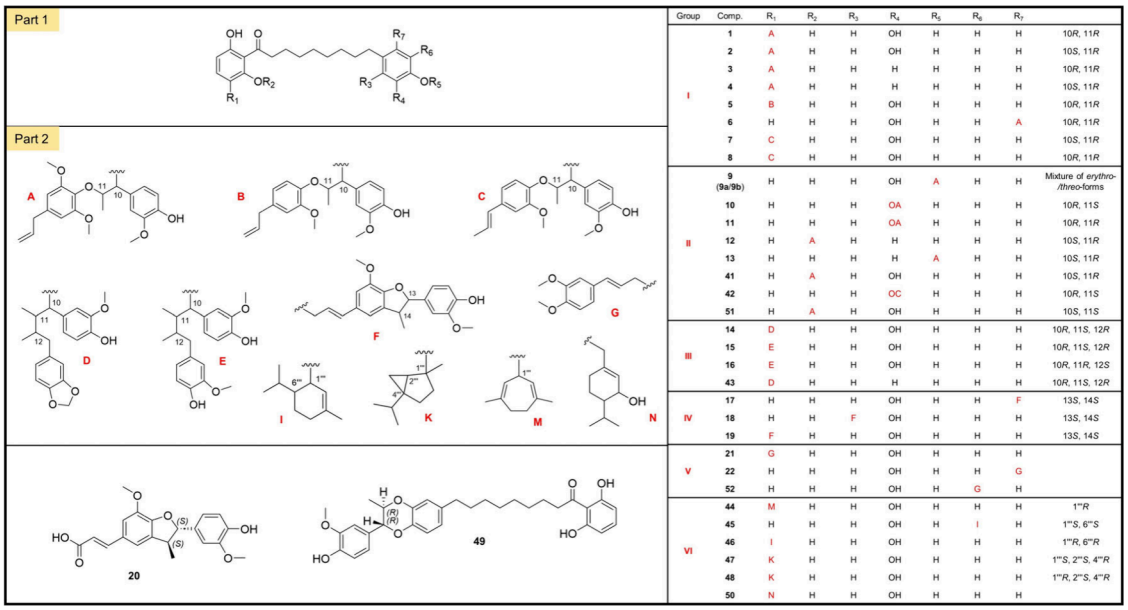

Group	Comp.	R_1	R_2	R_3	R_4	R_5	R_6	R_7	
I	1	A	H	H	OH	H	H	H	10*R*, 11*R*
	2	A	H	H	OH	H	H	H	10*S*, 11*R*
	3	A	H	H	H	H	H	H	10*R*, 11*R*
	4	A	H	H	H	H	H	H	10*S*, 11*R*
	5	B	H	H	OH	H	H	H	10*R*, 11*R*
	6	H	H	H	OH	H	H	A	10*R*, 11*R*
	7	C	H	H	OH	H	H	H	10*S*, 11*R*
	8	C	H	H	OH	H	H	H	10*R*, 11*R*
II	9 (9a/9b)	H	H	H	OH	A	H	H	Mixture of *erythro-* /*threo*-forms
	10	H	H	H	OA	H	H	H	10*R*, 11*S*
	11	H	H	H	OA	H	H	H	10*R*, 11*R*
	12	H	A	H	H	H	H	H	10*S*, 11*R*
	13	H	H	H	H	A	H	H	10*S*, 11*R*
	41	H	A	H	OH	H	H	H	10*S*, 11*R*
	42	H	H	H	OC	H	H	H	10*R*, 11*S*
	51	H	A	H	OH	H	H	H	10*S*, 11*S*
III	14	D	H	H	OH	H	H	H	10*R*, 11*S*, 12*R*
	15	E	H	H	OH	H	H	H	10*R*, 11*S*, 12*R*
	16	E	H	H	OH	H	H	H	10*R*, 11*R*, 12*S*
	43	D	H	H	H	H	H	H	10*R*, 11*S*, 12*R*
IV	17	H	H	H	OH	H	H	F	13*S*, 14*S*
	18	H	H	F	OH	H	H	H	13*S*, 14*S*
	19	F	H	H	OH	H	H	H	13*S*, 14*S*
V	21	G	H	H	OH	H	H	H	
	22	H	H	H	OH	H	H	G	
	52	H	H	H	OH	H	G	H	
VI	44	M	H	H	OH	H	H	H	1‴*R*
	45	H	H	H	OH	H	I	H	1‴*S*, 6‴*S*
	46	I	H	H	OH	H	H	H	1‴*R*, 6‴*R*
	47	K	H	H	OH	H	H	H	1‴*S*, 2‴*S*, 4‴*R*
	48	K	H	H	OH	H	H	H	1‴*R*, 2‴*S*, 4‴*R*
	50	N	H	H	OH	H	H	H	

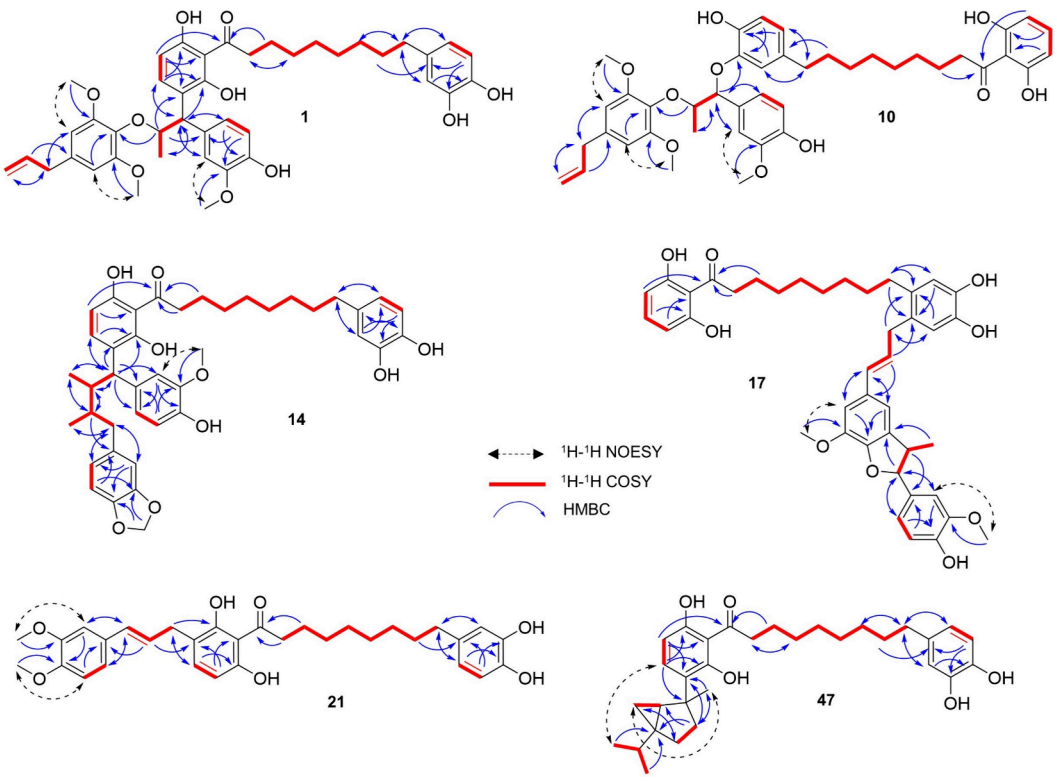

Figure 1. Key NOESY (black dash), COSY (red bold), and HMBC (blue arrows) correlations of representative compounds **1**, **10**, **14**, **17**, **21**, and **47**.

new 1,4-benzodioxane neolignan (**49**), and 31 new diarylnonanoid derivatives (**2**−**7**, **9**−**19**, **21**, **22**, **41**−**48**, and **50**−**52**), as well as known compounds (**1**, **8**, and **23**−**40**) (Figure S.36). The compounds (**1**−**19**, **21**−**22**, **41**−**48**, and **50**−**52**) isolated in this study were categorized into six groups (I−VI) based on the manner in which structural part 2 was substituted in structural part 1 and the specific properties of part 2 (see Chart 1, Figures S.51−S.53). In this paper, we provide structure determination for one representative compound from each group, and those of the other compounds can be found in the Supporting Information.

Myricone A (**1**) is also known as myrifragranone B[19] and was obtained as a yellowish gum with a molecular formula of $C_{42}H_{50}O_{10}$ from the ion peak at m/z 737.3302 $[M + Na]^+$ in the positive ion HRESIMS (calcd. for $C_{42}H_{50}O_{10}Na$, 737.3302). For part 1, the NMR spectrum showed signals of an asymmetric 1,2,3,6-tetrasubstituted benzene ring [δ_H 7.20 (1H, d, J = 8.5 Hz, H-4′) and 6.46 (1H, d, J = 8.5 Hz, H-5′)], a set of 1,3,4-trisubstituted benzene rings [δ_H 6.69 (1H, d, J =

https://doi.org/10.1021/acsomega.4c05649
ACS Omega 2024, 9, 35170−35181

Table 1. ^{1}H and ^{13}C NMR Spectroscopic Data for Compounds 1, 10, 14, and 17 in $CDCl_3$ (δ in ppm, J in Hz)

	δ_C				δ_H			
position	17	14	10	1	17	14	10	1
1	208.26, C	208.70, C	208.33, C	209.44, C				
2	44.91, CH_2	44.93, CH_2	44.95, CH_2	45.17, CH_2	3.07, t (7.5)	3.07, t (7.5)	3.07, t (7.4)	3.18, m
3	24.59, CH_2	24.69, CH_2	24.69, CH_2	24.64, CH_2	1.65, m	1.65, m	1.64, m	1.68, p (7.4)
4	29.38, CH_2	29.36, CH_2	29.48, CH_2	29.27, CH_2	1.22 − 1.32, m[a]	1.24 − 1.38, m[a]	1.11 − 1.33, m[a]	1.22−1.37, m[a]
5	29.36, CH_2	29.32, CH_2	29.38, CH_2	29.21, CH_2				
6	29.32, CH_2	29.24, CH_2	29.38, CH_2	29.11, CH_2				
7	29.29, CH_2	28.98, CH_2	28.86, CH_2	28.86, CH_2				
8	31.12, CH_2	31.52, CH_2	31.47, CH_2	31.35, CH_2	1.51, m	1.54, m	1.38, m	1.53, p (7.2)
9	32.18, CH_2	35.26, CH_2	35.22, CH_2	35.11, CH_2	2.50, t (7.5)	2.47, m	2.33, t (7.4)	2.46, t (7.6)
10	130.71, CH	45.87, CH	86.04, CH	53.85, CH	6.27, m	4.18, d (11.9)	5.19, d (2.7)	4.21, d (6.5)
11	127.56, CH	36.94, CH	81.82, CH	80.28, CH	6.13, dt (15.8, 6.4)	2.26, m	4.46, qd (6.4, 2.7)	5.30, p (6.2)
12	35.79, CH_2	35.03, CH	12.79, CH_3	18.57, CH_3	3.39, d (6.5)	1.84, m	1.22, d (6.4)	1.17, d (6.1)
13	94.08, CH	41.99, CH_2	40.73, CH_2	40.51, CH_2	5.07, d (9.4)	2.47, m	3.31, d (6.8)	3.35, d (6.7)
14	45.76, CH	11.11, CH_3	137.35, CH	137.06, CH	3.42, m	0.74, d (6.7)	5.93, ddt (16.9, 10.1, 6.7)	5.96, ddt (16.9, 10.2, 6.7)
15	17.82, CH_3	13.33, CH_3	116.29, CH_2	116.16, CH_2	1.34, d (6.7)	0.85, d (6.8)	5.08, m	5.13, m
1′	110.26, C	109.98, C	110.29, C	111.98, C				
2′	161.45, C	161.51, C	161.56, C	158.73, C				
3′	108.60, CH	125.47, C	108.48, CH	119.32, C	6.35, d (8.2)		6.35, d (8.2)	
4′	135.90, CH	134.08, CH	135.85, CH	138.38, CH	7.17, d (8.2)	7.14, d (8.5)	7.14, d (8.2)	7.20, d (8.5)
5′	108.60, CH	106.61, CH	108.48, CH	108.65, CH	6.35, d (8.2)	6.21, d (8.4)	6.35, d (8.2)	6.46, d (8.5)
6′	161.45, C	156.82, C	161.56, C	162.37, C				
1″	134.09, C	136.33, C	134.55, C	135.93, C				
2″	130.77, C	115.66, CH	118.25, CH	115.45, CH		6.70, d (2.0)	6.49, d (2.1)	6.69, d (2.0)
3″	116.96, CH	143.53, C	146.66, C	143.41, C	6.70, s			
4″	141.88, C	141.50, C	145.98, C	141.45, C				
5″	141.50, C	115.38, CH	115.53, CH	115.14, CH		6.77, m	6.82, d (8.1)	6.77, d (8.0)
6″	116.54, CH	120.97, CH	123.25, CH	120.70, CH	6.69, s	6.60, dd (8.0, 2.0)	6.65, dd (8.2, 2.0)	6.59, dd (8.0, 2.0)
1‴	132.04, C	136.28, C	131.07, C	132.45, C				
2‴	109.77, CH	111.15, CH	109.49, CH	111.60, CH	6.76, s	6.68, d (1.9)	7.04, d (1.9)	6.89, s
3‴	144.30, C	146.53, C	146.85, C	146.32, C				
4‴	146.89, C	143.70, C	145.14, C	144.03, C				
5‴	133.55, C	114.34, CH	114.38, CH	114.08, CH		6.79, d (8.2)	6.89, d (8.1)	6.87, s
6‴	113.87, CH	120.66, CH	119.97, CH	121.26, CH	6.76, s	6.65, dd (8.1, 1.9)	6.86, dd (8.2, 1.8)	6.87, s
1⁗	132.18, C	135.54, C	133.24, C	131.48, C				
2⁗	109.15, CH	109.62, CH	153.62, C	153.16, C	6.93, s	6.55, m		
3⁗	146.92, C	147.55, C	105.56, CH	105.23, CH			6.38, s	6.39, s
4⁗	146.00, C	145.63, C	136.34, C	136.61, C				
5⁗	114.34, CH	108.12, CH	105.56, CH	105.23, CH	6.87, s	6.75, d (7.7)	6.38, s	6.39, s
6⁗	120.16, CH	122.08, CH	153.62, C	153.16, C	6.87, s	6.53, m		
16	56.24, CH_3	100.90, CH_2	56.24, CH_3	55.86, CH_3	3.85, s	5.95, s	3.86, s	3.80, s
17	56.20, CH_3	56.00, CH_3	56.12, CH_3	55.86, CH_3	3.84, s	3.79, s	3.73, s	3.73, s
18			56.12, CH_3	55.86, CH_3			3.73, s	3.73, s

[a]Overlapped.

2.0 Hz, H-2″), 6.77 (1H, d, J = 8.0 Hz, H-5″), and 6.59 (1H, dd, J = 8.0, 2.0 Hz, H-6″)], an alkyl chain with eight methylene groups, one flanking the carbonyl group [δ_H 3.18 (2H, m, H-2), δ_C 45.17], one benzylic [δ_H 2.46 (2H, t, J = 7.6 Hz, H-9), δ_C 35.11], and six others [δ_H 1.68 (2H, p, J = 7.4 Hz, H-3), δ_C 24.64; δ_H 1.53 (2H, p, J = 7.2 Hz, H-8), δ_C 31.35; δ_H 1.22−1.37 (8H, m, H-4−7)], and a carbonyl group (δ_C 209.44). The association between the two aromatic rings via the alkyl chain and carbonyl groups was established by analyzing the HMBC spectrum (Figure 1). The ^{1}H NMR spectrum of part 2 contained the characteristic resonances for a set of 1,3,4-trisubstituted benzene rings [δ_H 6.89 (1H, s, H-2‴) and 6.87 (2H, s, H-5‴,6‴)], three methoxy groups [δ_H 3.80 (3H, s, H-16) and 3.73 (6H, s, H-17,18)], a methyl group [δ_H 1.17 (3H, d, J = 6.1 Hz, H-12)], two methines [δ_H 4.21 (1H, d, J = 6.5 Hz, H-10), 5.30 (1H, p, J = 6.2 Hz, H-11)], and a monosubstituted olefin [δ_H 5.13 (2H, m, H-15), 5.96 (1H, ddt, J = 16.9, 10.2, 6.7 Hz, H-14)]. The linkage of a propyl moiety between the two benzene rings and an allyl group was established from the HMBC cross-peaks (Figure 1). The positions of the methoxy groups were characterized by using HMBC correlations and supported by NOESY experiments (Figure 1). Finally, part 1 was revealed to be attached to part 2 via the connection between C-10 and C-3′, as confirmed by

https://doi.org/10.1021/acsomega.4c05649
ACS Omega 2024, 9, 35170−35181

HBMC cross-peaks of H-10 with C-2′ and C-4′ (Figure 1). When the ^{1}H NMR spectroscopic data for **1** were acquired using deuteriochloroform as the solvent, protons H-2‴, H-5‴, and H-6‴ were not distinguishable and appeared as two singlets at chemical shifts of 6.89 (1H) and 6.87 ppm (2H). The absence of coupling between these signals and the fact that H-5‴ and H-6‴ had identical chemical shifts could lead to an incorrect identification of a 1,3,5-trisubstituted benzene ring instead of a 1,3,4-trisubstituted benzene ring, as reported in the literature.[20,21] To verify the structure, additional NMR spectra of **1** were obtained by using acetone-d_6 as the solvent, which allowed for the differentiation of all aromatic protons (Table S.11). Collectively, the use of one- and two-dimensional NMR (COSY, HSQC, HMBC, and NOESY) permitted assignments of all the ^{1}H and ^{13}C signals for **1** (Table 1). In addition, a planar structure of **1** was determined, in an agreement with the planar structure of myrifragranone B reported by Oanh et al.[19] However, the determination of the relative configuration of **1** as the *threo*-form through the NOESY correlation between H-10 and H-12, as described in the aforementioned report, was found to be incorrect because of the spatial proximity of these protons. This was further proven because the NOESY correlation between H-10 and H-12 was also observed in **2** (*erythro*-form). Next, we identified the relative configuration of **1** using Maestro 10.6 for the coupling constant prediction of all possible relative configurations of **1**. The predicted J value between H-10 and H-11 protons (J_{10-11}= 5.0 Hz, Figure S.42) showed a very good correspondence with the observed experimental value (J_{10-11}= 6.5 Hz, Table 1). Thus, the relative configuration of **1** was established as the *threo*-form. This finding is consistent with those of previous studies that used large or small coupling constants in $CDCl_3$ to ascertain the relative configuration.[22,23] The absolute configuration of **1** was established on the basis of ECD spectroscopic evidence. The experimental ECD spectrum fit the calculated spectrum for the 10*R*,11*R*-configuration of simplified-**1** well (Figure S.43). Based on the above evidence, the structure of **1** is shown in Chart 1.

Myricone K (**10**) was obtained as a yellowish gum with a molecular formula of $C_{42}H_{50}O_{10}$ from the ion peak at m/z 737.3301 $[M + Na]^+$ in the positive ion HRESIMS (calcd. for $C_{42}H_{50}O_{10}Na$, 737.3302). Similar to compounds in group I, the ^{1}H and ^{13}C NMR data of **10** revealed the presence of a diphenylnonanoid group (part 1) and two phenylpropyl groups (part 2) (Tables S.3 and S.4). However, part 1 of **10** was connected to part 2 via an oxygen atom between C-10 and C-3″, as confirmed by the presence of an HMBC cross-peak of H-10 (δ_H 5.19) with C-3″ (δ_C 146.66) (Figure 1). The detected downfield chemical shift of H-10 (δ_H 5.19) and C-10 (δ_C 86.04) in **10** indicated a connection to oxygen rather than to the benzene ring. The relative configuration of **10** was determined to be the *erythro*-form based on the observed small J_{10-11} coupling constant of 2.7 Hz in the ^{1}H NMR spectrum (Figure S.42). Moreover, a comparison between the experimental ECD spectrum and the calculated spectrum for the 10*R*,11*S*-configuration of simplified-**10** (Figure S.44) revealed compelling evidence of their similarity. These findings provide conclusive evidence of the structure of **10**, as shown in Chart 1.

Myricone O (**14**) was obtained as a yellowish gum with a molecular formula of $C_{41}H_{48}O_9$ from the ion peak at m/z 707.3196 $[M + Na]^+$ in the positive ion HRESIMS (calcd. for $C_{41}H_{48}O_9Na$, 707.3196). The ^{1}H and ^{13}C NMR data of **14** revealed the presence of a diphenylnonanoid moiety (part 1), similar to those of compounds in groups I and II. However, **14** was found to contain a 2,3-dimethylbutane-type lignan unit (part 2) instead of the two phenylpropyl groups. In addition, the signals of the 2,3-dimethylbutane-type lignan unit of **14** are similar to those of myristargenol A (Table 1).[24] This similarity was validated by observing signals of two sets of 1,3,4-trisubstituted benzene ring [δ_H 6.68 (1H, d, J = 1.9 Hz, H-2‴), 6.79 (1H, d, J = 8.2 Hz, H-5‴), and 6.65 (1H, dd, J = 8.1, 1.9 Hz, H-6‴)] and [δ_H 6.55 (1H, m, H-2⁗), 6.75 (1H, d, J = 7.7 Hz, H-5⁗), and 6.53 (1H, m, H-6⁗)], two methyl groups [δ_H 0.74 (3H, d, J = 6.7 Hz, H-14) and 0.85 (3H, d, J = 6.8 Hz, H-15)], three methines [δ_H 4.18 (1H, d, J = 11.9 Hz, H-10), 2.26 (1H, m, H-11), and 1.84 (1H, m, H-12)], one methylene [δ_H 2.47 (2H, m, H-13)], one methoxy group [δ_H 3.79 (3H, s, H-17)], and one methylenedioxy group [δ_H 5.95 (2H, s, H-16)]. The linkage between C-10 and C-3′, as validated by the HMBC cross-peak of H-10 (δ_H 4.18) with C-2′ (δ_C 161.51) and C-4′ (δ_C 134.08), established the correlation between parts 2 and 1 (Figure 1). The relative rigidity of the molecule was attributed to the *anti*-periplanar alignment between H-10 and H-11, which was revealed by applying the Karplus equation to the coupling constant (J = 11.9 Hz).[25] The coupling constant between H-11 and H-12 was initially predicted to be approximately 2.5 Hz by NMR simulation (Figure S.37) and further determined to be 2.2 Hz (Figure S.38) by selective homonuclear decoupled ^{1}H NMR experiments, suggesting the *gauche* correlation between H-11 and H-12. Thus, based on the NOESY data (Figure S.38), the relative configurations of **14** were proposed as *rel*-10*S*,11*R*,12*S*. Finally, the absolute configuration of **14** was determined by comparing calculated and experimental ECD spectra (Figure S.45), and the structure of **14** is as shown in Chart 1.

Myricone Q (**17**) was isolated as a yellowish gum with a molecular formula of $C_{41}H_{46}O_9$ from the ion peak at m/z 705.3040 $[M + Na]^+$ in the positive ion HRESIMS (calcd. for $C_{41}H_{46}O_9Na$, 705.3040). The ^{1}H and ^{13}C NMR data of **17** indicated the presence of a diphenylnonanoid group (part 1), akin to that observed in compounds of groups I, II, and III. However, **17** exhibited a dihydrobenzofuran neolignan moiety (part 2) instead of two phenylpropyl groups. The signals of the dihydrobenzofuran neolignan moiety of **17** are similar to those of **20** (Table 1), and structural determination was achieved after detecting signals of a pair of *meta*-coupled aromatic protons [δ_H 6.76 (2H, s, H-2‴,6‴)], an ABX system [δ_H 6.93 (1H, s, H-2⁗)], 6.87 (2H, s, H-5⁗,6⁗)], two methine protons [δ_H 5.07 (1H, d, J = 9.4 Hz, H-13) and 3.42 (1H, m, H-14)], one methyl proton [δ_H 1.34 (3H, d, J = 6.7 Hz, H-15)], a disubstituted *trans*-olefin [δ_H 6.27 (1H, m, H-10) and 6.13 (1H, dt, J = 15.8, 6.4, H-11)], and two methoxy groups [δ_H 3.85 (3H, s, H-16) and 3.84 (3H, s, H-17)]. The locations of the methoxy groups were characterized by NOESY experiments, which revealed NOE correlations between H-17 (δ_H 3.84) and H-2⁗ (δ_H 6.93), as well as H-16 (δ_H 3.85) and H-2‴ (δ_H 6.76) (Figure 1). Further, part 2 was connected to part 1 via C-12 and C-2″, as confirmed by the HBMC cross-peak of H-12 (δ_H 3.39) with C-1″ (δ_C 134.09) and C-3″ (δ_C 116.96) (Figure 1). As for **1**, **17** was analyzed by NMR in acetone-d_6, which enabled the identification of more aromatic protons (Table S.15). In the dihydrobenzofuran ring, the large vicinal coupling constant (J = 9.4 Hz) between H-13 and H-14 indicates a *trans*-relative configuration for these methine protons.[26,27] The absolute configuration of **17** was determined

https://doi.org/10.1021/acsomega.4c05649
ACS Omega 2024, 9, 35170−35181

as 13*S*,14*S* from the positive Cotton effect at 241 nm in the ECD spectrum, which is in contrast to that of 3′-methoxylicarin B (Figure S.46).[27,28] Therefore, the structure of compound **17** was elucidated, as shown in Chart 1.

Myricone Z (**21**) was obtained as a yellowish gum with a molecular formula of $C_{32}H_{38}O_7$ from the ion peak at *m*/*z* 557.2515 $[M + Na]^+$ in the positive ion HRESIMS (calcd. for $C_{32}H_{38}O_7Na$, 557.2515). The NMR data for **21** (Table 2)

Table 2. ^{1}H and ^{13}C NMR Spectroscopic Data for Compounds 21 and 47 in $CDCl_3$ (δ in ppm, *J* in Hz)

	δ_H		δ_C	
position	**21**	**47**	**21**	**47**
1	208.49, C	208.84, C		
2	45.04, CH_2	45.09, CH_2	3.09, t (7.4)	3.09, t (7.4)
3	24.65, CH_2	24.81, CH_2	1.66, m	1.67, m
4	29.38, CH_2	29.43, CH_2	1.21−1.36, m[a]	1.22 − 1.39, m[a]
5	29.37, CH_2	29.39, CH_2		
6	29.28, CH_2	29.28, CH_2		
7	29.02, CH_2	29.01, CH_2		
8	31.55, CH_2	31.56, CH_2	1.51, m	1.53, m
9	35.29, CH_2	35.28, CH_2	2.45, t (7.6)	2.47, t (7.6)
10	131.34, CH	32.04, CH	6.41, d (15.8)	1.52, m
11	126.18, CH	20.56, CH_3	6.20, dt (15.8, 6.7)	0.82, d (6.8)
12	33.40, CH_2	20.20, CH_3	3.46, d (6.7)	0.82, d (6.8)
13	56.16, CH_3	23.95, CH_3	3.85, s	1.42, s
14	56.04, CH_3		3.84, s	
1′	110.29, C	110.29, C		
2′	160.44, C	162.85, C		
3′	119.06, C	128.67, C		
4′	136.48, CH	133.50, CH	7.15, d (8.3)	7.32, d (8.5)
5′	107.43, CH	105.24, CH	6.30, d (8.2)	6.17, d (8.5)
6′	158.91, C	156.59, C		
1″	136.32, C	136.46, C		
2″	115.67, CH	115.73, CH	6.66, d (2.0)	6.69, d (1.9)
3″	143.53, C	143.48, C		
4″	141.49, C	141.38, C		
5″	115.39, CH	115.45, CH	6.73, d (8.1)	6.75, d (8.0)
6″	121.01, CH	121.08, CH	6.57, dd (8.1, 2.0)	6.59, dd (8.0, 2.0)
1‴	130.50, C	45.37, C		
2‴	108.87, CH	32.74, CH	6.89, d (2.0)	1.50, m
3‴	149.19, C	9.74, CH_2		0.44, t (4.4)
				0.32, dd (8.4, 5.0)
4‴	148.78, C	34.71, C		
5‴	111.38, CH	28.18, CH_2	6.78, d (8.2)	1.53/1.38, m
6‴	119.52, CH	33.61, CH_2	6.87, dd (8.2, 2.0)	2.09/1.18, m

[a]Overlapped.

revealed that the signals of part 1 are similar to those of part 1 of **1**. For part 2, the ^{1}H NMR spectrum contains signals for a set of 1,3,4-trisubstituted benzene rings [δ_H 6.89 (1H, d, *J* = 2.0 Hz, H-2‴), 6.78 (1H, d, *J* = 8.2 Hz, H-5‴), and 6.87 (1H, dd, *J* = 8.2, 2.0 Hz, H-6‴)], two methoxy groups [δ_H 3.85 (3H, s, H-13) and 3.84 (3H, s, H-14)], and a disubstituted *trans*-olefin [δ_H 6.41 (1H, d, *J* = 15.8 Hz, H-10) and 6.20 (1H, dt, *J* = 15.8, 6.7 Hz, H-11)]. Finally, we found that part 2 was connected to part 1 via the NOE correlations between H-12 (δ_H 3.46) and C-2′ (δ_C 160.44), C-4′ (δ_C 136.48) (Figure 1). The positions of the methoxy groups were confirmed from the HBMC correlations between H-13 (δ_H 3.85) and C-3‴ (δ_C 149.19) and between H-14 (δ_H 3.84) and C-4‴ (δ_C 148.78) (Figure 1) and reconfirmed through a NOESY experiment, which revealed the correlations between H-13 (δ_H 3.85) and H-2‴ (δ_C 108.87), as well as between H-14 (δ_H 3.84) and H-5‴ (δ_C 111.38) (Figure 1). Consequently, the structure of **21** was determined and is displayed in Chart 1.

Myfracone D (**47**) was isolated as a yellowish gum with a molecular formula of $C_{31}H_{42}O_5$ from the ion peak at *m*/*z* 517.2929 $[M + Na]^+$ in the positive-ion HRESIMS (calculation for $C_{31}H_{42}O_5Na$, 517.2930). Belonging to group VI, which includes monoterpene-diarylnonanoid conjugates, the monoterpene moiety of **47** displayed characteristic resonances for three methylene groups [δ_H 0.44 (1H, t, *J* = 4.4 Hz, H-3‴a), 0.32 (1H, dd, *J* = 8.4, 5.0 Hz, H-3‴b), δ_C 9.74; δ_H 1.53/1.38 (2H, m, H-5‴), δ_C 28.18; δ_H 2.09/1.18 (2H, m, H-6‴), δ_C 33.61], two methines [δ_H 1.50 (1H, m, H-2‴), δ_C 32.74; δ_H 1.52 (1H, m, H-10), δ_C 32.04], and three methyl groups [δ_H 0.82 (3H, d, *J* = 6.8 Hz, H-11), δ_C 20.56; δ_H 0.82 (3H, d, *J* = 6.8 Hz, H-12), δ_C 20.20; δ_H 1.42 (3H, s, H-13), δ_C 23.95]. Part 1 was demonstrated to be connected to part 2 via the C-1‴/C-3′ linkage, which was verified by detecting HBMC cross-peaks between C-1‴′ (δ_C 45.37) and H-4′ (δ_H 7.32) (Figure 1). The relative configuration of **47** was determined to be *rel*-1‴*S*,2‴*S*,4‴*R* based on observed NOE correlations between H-4′ (δ_H 7.32) and H-11 (δ_H 0.82), H-12 (δ_H 0.82) as well as H-3‴a (δ_H 0.44) and H-13 (δ_H 1.42) (Figure 1). Afterward, we established the absolute configuration of **47** by comparing its experimental ECD spectrum with the calculated spectrum for the 1‴*S*,2‴*S*,4‴*R*-configuration of simplified-**47**. This analysis confirmed its absolute configuration as 1‴*S*,2‴*S*,4‴*R* (Figure S.47). As a result, we finalized the structural assignment of **47**, as outlined in Chart 1.

In terms of initial biological activity, the isolated compounds were initially assessed for their impact on the viability of RAW 264.7 cells using the MTT assay (Figure S.54). The results indicated that compounds **1**, **3**, **5**, **6**, **8**, **10**, **15**, and **21** significantly affected cell viability, while compounds **2**, **4**, **9**, **11**, **12**, **14**, and **17**−**20** showed no significant effect on cell viability. Therefore, a concentration of 12.5−50 μM of compounds **2**, **4**, **9**, **11**, **12**, **14**, and **17**−**20** was selected for subsequent experiments, which evaluated effects of those compounds on NFkB/AP1, IRF activity, and proinflammatory cytokine and NO production. The investigation of compounds **2**, **4**, **9**, **11**, **12**, **14**, and **17**−**20** for their inhibitory effects on NF-κB/AP1 and IRF signaling pathways induced by the TLR agonists Pam3CSK4 (TLR2), Poly (IC) (TLR3), LPS (TLR4), FLA-ST (TLR5), and R848 (TLR7-8) yielded significant insights into their potential as therapeutic agents for modulating immune responses. We found that compounds **2**, **4**, **9**, **11**, **12**, **14**, **17**, and **18** exhibit notable dose-dependent inhibition of the NF-κB/AP1 signaling pathway when exposed to TLR2, TLR4, TLR7, and TLR8 agonists (Figure 2). This finding suggests that these compounds could effectively mitigate the activation of this pathway, which is a central regulator of proinflammatory cytokines and immune responses. Such inhibition could be valuable in the context of diseases characterized by excessive inflammation. Moreover, our results demonstrate that compounds **2**, **4**, **9**, **11**, **12**, **14**, **17**, and **18** also effectively inhibit the IRF signaling pathway when treated with TLR2, TLR3, TLR4, TLR5, TLR7, and TLR8 agonists (Figure 3). The dose-dependent manner of inhibition implies the potential for precise control over type I interferon production and downstream antiviral responses. This finding

https://doi.org/10.1021/acsomega.4c05649
ACS Omega 2024, 9, 35170−35181

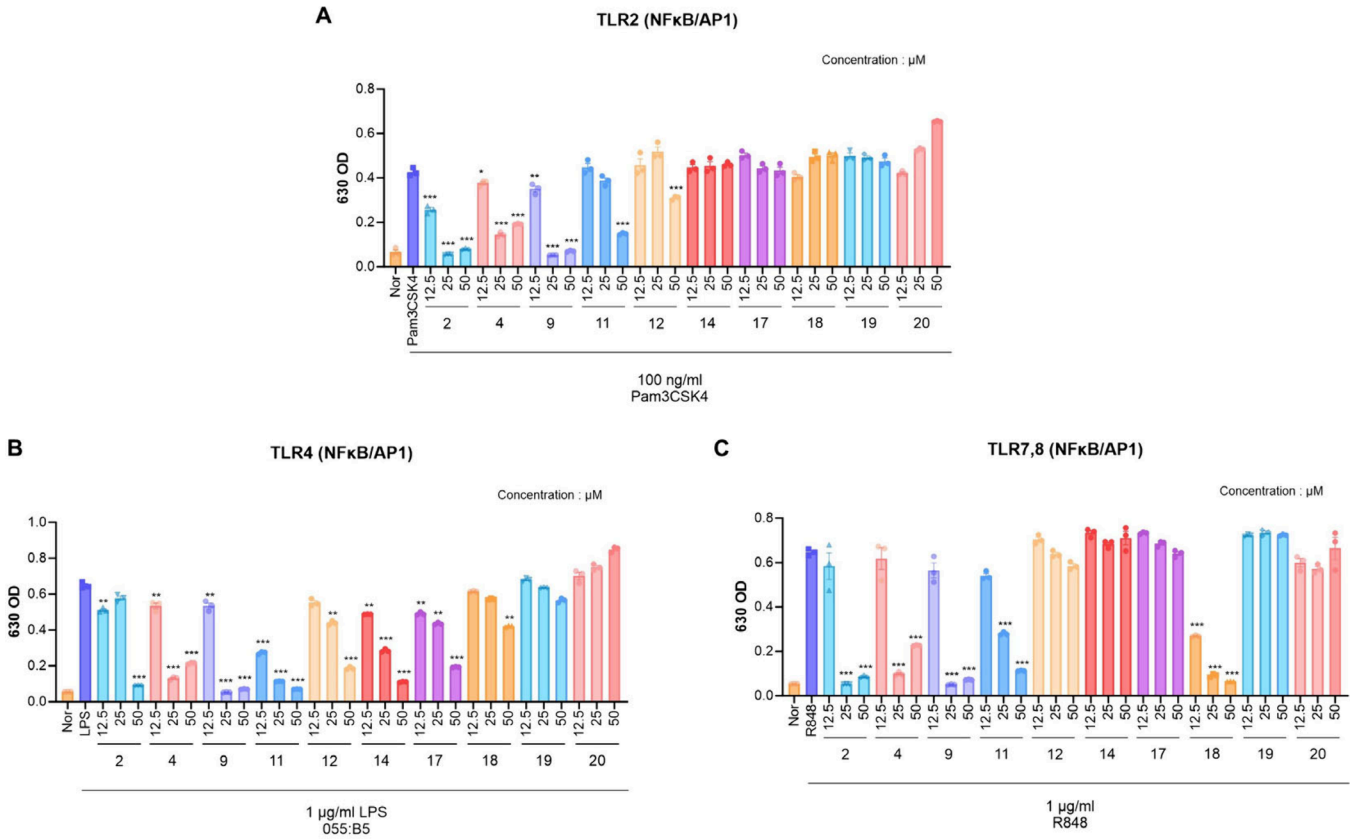

Figure 2. Effects of compounds on NFkB/AP1 activity. (A) NFkB/AP1 activity (100 ng/mL Pam3CSK4; TLR2 ligand), (B) NFkB/AP1 activity (1 μg/mL LPS; TLR4 ligand), and (C) NFkB/AP1 activity (1 μg/mL R848; TLR7,8 ligands). Experimental values are expressed as mean ± standard error of the mean values from three independent experiments (***$p < 0.001$).

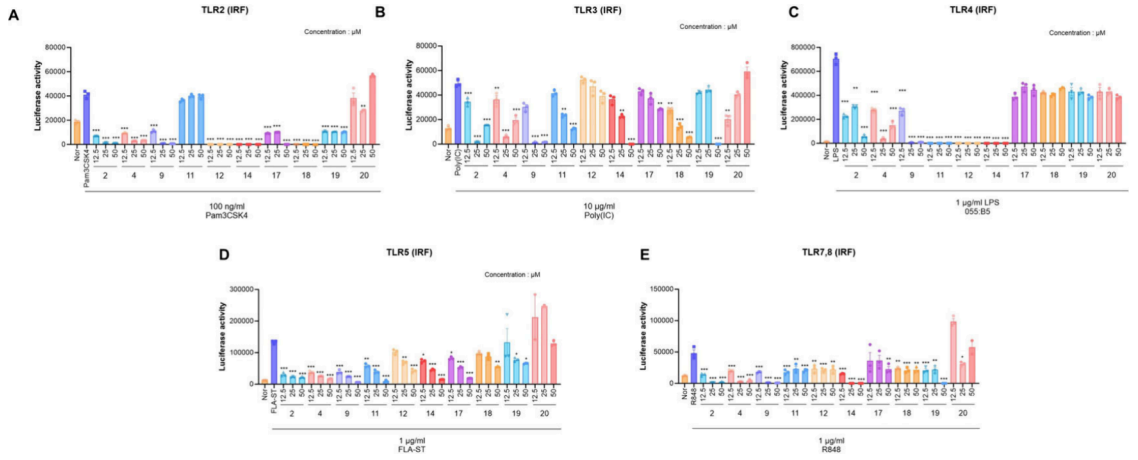

Figure 3. Effects of compounds on IRF activity: (A) IRF activity (100 ng/mL Pam3CSK4; TLR2 ligand), (B) IRF activity (10 μg/mL Poly (I:C); TLR3 ligand), (C) IRF activity (1 μg/mL LPS; TLR4 ligand), (D) IRF activity (1 μg/mL FLA-ST; TLR5 ligand), and (E) IRF activity (1 μg/mL R848; TLR 7,8 ligand). Experimental values are expressed as mean ± standard error of the mean values from three independent experiments (***$p < 0.001$).

underscores the versatility of these compounds in modulating immune reactions. Additionally, the assessment of the final products of these pathways (interleukin-6 and NO) revealed that compounds **2**, **4**, **6**, and **11** can inhibit the production of these proinflammatory mediators (Figure 4). The reduction in IL-6 levels suggests the potential dampening of the proinflammatory cytokine storm, which has a critical role in various inflammatory diseases. The inhibition of NO production is of significance because excessive NO release is associated with inflammation and tissue damage.

CONCLUSIONS

A total of 33 new compounds were isolated from the seeds of *M. fragrans*. These include 8-O-4′-neolignan-diarylnonanoid conjugates (groups I, II), 2,3-dimethylbutane-type lignan-diarylnonanoid conjugates (group III), dihydrobenzofuran neolignan-diarylnonanoid conjugates (group IV), propenyl-

https://doi.org/10.1021/acsomega.4c05649
ACS Omega 2024, 9, 35170−35181

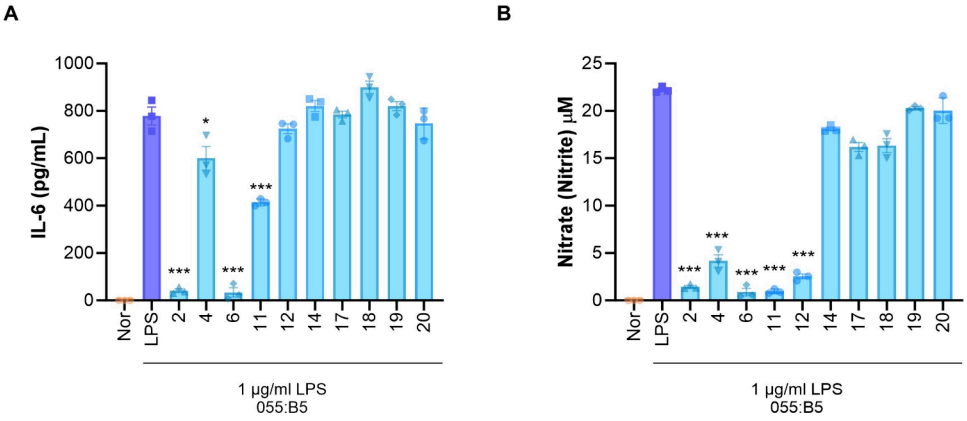

Figure 4. Effects of compounds on proinflammatory cytokine production and NO production. RAW 264.7 cells were pretreated with 50 μM compounds for 1 h and treated with 10 ng/mL LPS for 24 h. (A) The level of IL-6 induced by LPS in RAW 264.7 cells. (B) The level of nitric oxide induced by LPS in RAW 264.7 cells. Experimental values are expressed as mean ± standard error of the mean values from three independent experiments (*p < 0.05, ***p < 0.001).

benzene-diarylnonanoid conjugates (group V), and monoterpene-diarylnonanoid conjugates (group VI), along with two other neolignans (compounds **20** and **49**), and 20 known compounds (compounds **1**, **8**, and **23**−**40**). Compounds **2**, **4**, **9**, **11**, **12**, **14**, **17**, and **18** demonstrated promising inhibitory effects on NF-κB/AP1 and IRF signaling pathways induced by TLR agonists (data summarized in Table S.16). Notably, different behavior was observed for the stereoisomers, particularly within the subset of group-I compounds. Specifically, although the 10*R*,11*R*-isomers (**1**, **3**, **5**, **6**, and **8**) exhibited cytotoxicity leading to cell death, the 10*S*,11*R*-isomers (**2** and **4**) yielded the opposite effect (Figure S.54). Together, these findings significantly enrich the chemical diversity of *M. fragrans* and suggest the potential of these compounds as therapeutics for conditions characterized by dysregulated immune responses and inflammation. However, further studies are required to elucidate the precise mechanisms of action and evaluate their safety and efficacy in in vivo models. Nonetheless, the findings of this study provide valuable insights into the development of targeted immunomodulatory interventions.

EXPERIMENTAL PROCEDURES

General Experimental Procedures. Optical rotations were measured with a PerkinElmer Model 343 polarimeter. UV spectra were acquired by using a PerkinElmer Lambda 35 UV/vis spectrophotometer. ECD spectra were acquired on a Chirascan V100 spectropolarimeter. IR spectra were obtained by using a Thermo Scientific Nicolet iS10 FT-IR spectrometer. The NMR spectra (^{1}H, ^{13}C, ^{1}H−^{1}H COSY, HSQC, HMBC, and NOESY) were obtained using a Varian 500 MHz NMR spectrometer and Bruker AVANCE III HD 800 NMR spectrometer equipped with a 5 mm TCI CryoProbe operating at 850 MHz. The HRESIMS data were acquired on a Waters SYNAPT G2 (Waters, Milford, MA, USA) mass spectrometer. HPLC chromatograms and ESIMS data were obtained using an Agilent 1200 system connected to a 6120 quadrupole MSD with a Triart YMC C18 column (3 μm, 250 × 4.6 mm). Preparative MPLC was carried out using a YMC MPLC system with a YMC ODS column (5 μm, 250 × 20 mm). Open columns were filled with normal-phase silica gel 60 (70−230; Merck, Darmstadt, Germany). Thin layer chromatography (TLC) was conducted using precoated silica gel F254 plates for normal-phase separation. Spots were visualized either under UV light or by heating the plates after spraying them with 10% sulfuric acid.

Plant Material. The nutmegs of *M. fragrans* from Indonesia were purchased from a commercial market (Dongkwang, Seoul, Korea) in 2023. The sample was authenticated by Prof. Sang Hoon Jung (one of the authors), and a voucher specimen (KISTMF-0223) was deposited at the Natural Product Center, Korea Institute of Science and Technology, Gangwon-do, Republic of Korea.

Extraction and Isolation. The dried nutmegs of *M. fragrans* (5.0 kg) were extracted with 75% aqueous EtOH at room temperature, and the extract was filtered and concentrated to yield an EtOH extract (205 g), which was suspended in distilled water and sequentially partitioned with methylene chloride (MC) and ethyl acetate (EA) to obtain residues of 100 and 2 g, respectively. The MC-soluble fraction (100 g) was fractionated over a silica gel column (hexanes−EA, 20:1 → 100% EA) to furnish 30 fractions (MFMC-1−30). Small portions (50 mg) of fraction MFMC-1 (10.2 g), fraction MFMC-4 (3.4 g), and fraction MFMC-10 (2.3 g) were subjected to preparative MPLC utilizing acetonitrile (ACN)/H_2O (gradient, flow rate 5 mL/min, YMC C18 column) to yield myristicin[8,28,29] (**33**, 12.1 mg), methyleugenol[8,29,30] (**36**, 3.2 mg), and 3′-methoxylicarin B[27] (**30**, 15.3 mg), respectively; myristic acid[31] (**31**, 8.2 mg) was precipitated and collected from fraction MFMC-9 (2.1 g) using MeOH as the solvent for the precipitation. Similar to **31**, β-sitosterol[32] (**29**, 6.1 mg) was separated from fraction MFMC-13 (500 mg). Fraction MFMC-21 (3.2 g) was applied to a Sephadex LH-20 column eluted with MeOH−H_2O (2:10 → 100% MeOH) to produce six subfractions (21-1 to 21-6). *trans*-3,4,5-Trimethoxycinnamic alcohol[32] (**32**, 2.1 mg), *trans*-3,4-dimethoxyeinnamyl alcohol[33] (**34**, 3.4 mg), and anthriscinol[34] (**35**, 2.1 mg) were acquired by purifying subfraction 21−2 (120 mg) using preparative MPLC with ACN/H_2O (gradient, flow rate 5 mL/min). Subfraction 21-5 was applied again to a Sephadex LH-20 column eluted with MeOH−H_2O (3:10 → 100% MeOH) to obtain 67 subfractions (21-5-1 to 21-5-67). Myricone E (**5**, 4.2 mg), myricone F (**6**, 6.2 mg), giganteone A[35] (**26**, 3.1 mg), giganteone B[35] (**28**, 2.3 mg), and giganteone C[36] (**27**, 2.1 mg) from subfraction 21-5-61, myricone A or myrifragranone B[19] (**1**, 46.2 mg), myricone B (**2**, 34.8 mg), myricone C (**3**, 21.6

https://doi.org/10.1021/acsomega.4c05649
ACS Omega 2024, 9, 35170−35181

mg), myricone D (**4**, 13.3 mg), myricone G (**7**, 1.3 mg), myrifragranone A[19] (**8**, 4.3 mg), malabaricone B[9,37] (**23**, 19.1 mg), and malabaricone C[9,37] (**24**, 113.3 mg) from subfraction 21-5-63, the mixture of myricone H, I (**9a** and **9b**, 11.5 mg), myricone K (**10**, 5.3 mg), myricone L (**11**, 6.4 mg), myricone M (**12**, 5.7 mg), and myricone N (**13**, 1.4 mg) from subfraction 21-5-65; myricone O (**14**, 7.5 mg), myricone P (**15**, 7.3 mg), myricone R (**16**, 1.2 mg), myricone Q (**17**, 3.1 mg), myricone T (**18**, 3.3 mg), myricone X (**19**, 2.9 mg), myricone Z (**21**, 2.1 mg), and myricone W (**22**, 1.1 mg) from subfraction 21-5-60, myrifratin D[38] (**38**, 1.6 mg), myrifratin E[38] (**39**, 1.8 mg), malabaricone A[39] (**40**, 2.9 mg), myricone J (**41**, 5.6 mg), myricone S (**42**, 1.6 mg), and myricone U (**43**, 2.3 mg) from subfraction 21-5-57, myfracone G (**50**, 1.7 mg), myfracone H (**51**, 1.9 mg), and myfracone I (**52**, 0.7 mg) from subfraction 21-5-58 were purified using preparative MPLC with ACN/H_2O (isocratic, 70% ACN, flow rate 8 mL/min). Fraction MFMC-28 (550 mg) was separated on a Sephadex LH-20 column eluted with MeOH−H_2O (3:10 → 100% MeOH), then purified using preparative MPLC with ACN/H_2O (gradient, flow rate 5 mL/min) to afford *trans*-3,4-dimethoxycinnamic acid[40] (**37**, 2.5 mg), promalabaricone B[37] (**25**, 1.9 mg), and myricone Y (**20**, 2.2 mg). Finally, fraction MFMC-29 (720 mg) was separated on a Sephadex LH-20 column eluted with MeOH−H_2O (7:3 → 100% MeOH), then purified using preparative MPLC with ACN/H_2O (isocratic, 85% ACN, flow rate 8 mL/min) to collect myfracone A (**44**, 2.1 mg), myfracone B (**45**, 2.2 mg), myfracone C (**46**, 3.2 mg), myfracone D (**47**, 3.1 mg), myfracone E (**48**, 2.5 mg), and myfracone F (**49**, 3.7 mg). The known compounds were determined by comparing the spectroscopic data with the reported literature values.

*Myricone A (**1**):* yellowish gum; $[\alpha]^{20}_D$ +96 (*c* 0.02, MeOH); UV (MeOH) λ_{max} (log ε) 240 (3.09), 273 (3.01), and 353 (2.23) nm; IR (KBr) ν_{max} 3645, 3235, 2925, 2858, 1745, 1598, 1515, 1241, 1053, 1032, 755, and 689 cm^{-1}; ECD (MeOH) λ_{max} ($\Delta\varepsilon$) 238 (−18.03) and 273 (1.65) nm; ^{1}H NMR (500 MHz) and ^{13}C NMR (125 MHz) data in chloroform-*d* (Table 1), in acetone-d_6 (Table S.11); HRESIMS (positive-ion mode) *m*/*z* 737.3302 $[M + Na]^+$ (calcd. for $C_{42}H_{50}O_{10}Na$, 737.3302).

*Myricone B (**2**):* yellowish gum; $[\alpha]^{20}_D$ +83 (*c* 0.03, MeOH); UV (MeOH) λ_{max} (log ε) 240 (3.04), 273 (2.83), and 353 (2.08) nm; IR (KBr) ν_{max} 3680, 2924, 2862, 1600, 1515, 1228, 1054, 1033, and 689 cm^{-1}; ECD (MeOH) λ_{max} ($\Delta\varepsilon$) 238 (20.23) and 284 (3.45) nm; ^{1}H NMR (500 MHz) and ^{13}C NMR (125 MHz) data in chloroform-*d*, see Tables S.1 and S.2; HRESIMS (positive-ion mode) *m*/*z* 737.3301 $[M + Na]^+$ (calcd. for $C_{42}H_{50}O_{10}Na$, 737.3302).

*Myricone C (**3**):* yellowish gum; $[\alpha]^{20}_D$ +62 (*c* 0.02, MeOH); UV (MeOH) λ_{max} (log ε) 240 (2.95), 273 (2.56), and 353 (1.88) nm; IR (KBr) ν_{max} 3698, 2975, 2862, 1698, 1599, 1514, 1231, 1057, 1032, and 655 cm^{-1}; ECD (MeOH) λ_{max} ($\Delta\varepsilon$) 238 (−24.23) and 273 (2.44) nm; ^{1}H NMR (500 MHz) and ^{13}C NMR (125 MHz) data in chloroform-*d* (Tables S.1 and S.2), in acetone-d_6 (Table S.11); HRESIMS (positive-ion mode) *m*/*z* 721.3354 $[M + Na]^+$ (calcd. for $C_{42}H_{50}O_9Na$, 721.3353).

*Myricone D (**4**):* yellowish gum; $[\alpha]^{20}_D$ +56 (*c* 0.02, MeOH); UV (MeOH) λ_{max} (log ε) 240 (3.02), 273 (2.70), and 353 (1.98) nm; IR (KBr) ν_{max} 2924, 2855, 1744, 1601, 1513, 1261, 1055, 1032, and 655 cm^{-1}; ECD (MeOH) λ_{max} ($\Delta\varepsilon$) 238 (17.78) and 284 (2.53) nm; ^{1}H NMR (500 MHz) and ^{13}C NMR (125 MHz) data in chloroform-*d*, see Tables S.1 and S.2; HRESIMS (positive-ion mode) *m*/*z* 721.3352 $[M + Na]^+$ (calcd. for $C_{42}H_{50}O_9Na$, 721.3353).

*Myricone E (**5**):* yellowish gum; $[\alpha]^{20}_D$ +44 (*c* 0.02, MeOH); UV (MeOH) λ_{max} (log ε) 230 (2.56), 280 (2.26), and 351 (1.30) nm; IR (KBr) ν_{max} 2940, 2833, 1749, 1661, 1549, 1139, 1028, and 767 cm^{-1}; ECD (MeOH) λ_{max} ($\Delta\varepsilon$) 238 (−10.84) nm; ^{1}H NMR (500 MHz) and ^{13}C NMR (125 MHz) data in chloroform-*d* (Tables S.1 and S.2), in acetone-d_6 (Table S.12); HRESIMS (positive-ion mode) *m*/*z* 707.3198 $[M + Na]^+$ (calcd. for $C_{41}H_{48}O_9Na$, 707.3196).

*Myricone F (**6**):* yellowish gum; $[\alpha]^{20}_D$ +76 (*c* 0.03, MeOH); UV (MeOH) λ_{max} (log ε) 225 (3.06), 272 (2.74), and 340 (2.02) nm; IR (KBr) ν_{max} 2926, 2853, 1628, 1512, 1226, 1035, and 667 cm^{-1}; ECD (MeOH) λ_{max} ($\Delta\varepsilon$) 243 (−3.40) and 291 (2.91) nm; ^{1}H NMR (500 MHz) and ^{13}C NMR (125 MHz) data in chloroform-*d* see Tables S.1 and S.2; HRESIMS (positive-ion mode) *m*/*z* 737.3300 $[M + Na]^+$ (calcd. for $C_{42}H_{50}O_{10}Na$, 737.3302).

*Myricone G (**7**):* yellowish gum; $[\alpha]^{20}_D$ +19 (*c* 0.01, MeOH); UV (MeOH) λ_{max} (log ε) 230 (2.77), 270 (2.45), and 351 (1.54) nm; IR (KBr) ν_{max} 2924, 2861, 1748, 1600, 1513, 1278, 1054, and 1002 cm^{-1}; ECD (MeOH) λ_{max} ($\Delta\varepsilon$) 238 (+17.56) nm; ^{1}H NMR (500 MHz) and ^{13}C NMR (125 MHz) data in chloroform-*d* (Tables S.1 and S.2), in acetone-d_6 (Table S.12); HRESIMS (positive-ion mode) *m*/*z* 707.3195 $[M + Na]^+$ (calcd. for $C_{41}H_{48}O_9Na$, 707.3196).

*Myrifragranone A (**8**):* yellowish gum; $[\alpha]^{20}_D$ +23 (*c* 0.01, MeOH); ECD (MeOH) λ_{max} ($\Delta\varepsilon$) 239 (−7.86) nm; ^{1}H NMR (500 MHz) and ^{13}C NMR (125 MHz) data in chloroform-*d*, see Table S.10; HRESIMS (positive-ion mode) *m*/*z* 707.3195 $[M + Na]^+$ (calcd. for $C_{41}H_{48}O_9Na$, 707.3196).

*Mixture of Myricone H (**9a**) and Myricone I (**9b**):* yellowish gum; UV (MeOH) λ_{max} (log ε) 220 (2.67), 271 (2.02), and 340 (1.30) nm; IR (KBr) ν_{max} 2934, 2850, 1741, 1627, 1593, 1509, 1271, 1054, 1033, and 666 cm^{-1}; ^{1}H NMR (500 MHz) and ^{13}C NMR (125 MHz) data in chloroform-*d*, see Tables S.3 and S.4; HRESIMS (positive-ion mode) *m*/*z* 737.3300 $[M + Na]^+$ (calcd. for $C_{42}H_{50}O_{10}Na$, 737.3302).

*Myricone K (**10**):* yellowish gum; $[\alpha]^{20}_D$ +80 (*c* 0.02, MeOH); UV (MeOH) λ_{max} (log ε) 227 (2.93), 272 (2.71), and 340 (1.95) nm; IR (KBr) ν_{max} 2925, 2855, 1592, 1277, 1128, and 667 cm^{-1}; ECD (MeOH) λ_{max} ($\Delta\varepsilon$) 215 (−13.93), (+3.98), 244 (−6.97), and 274 (−3.09) nm; ^{1}H NMR (500 MHz) and ^{13}C NMR (125 MHz) data in chloroform-*d*, see Table 1; HRESIMS (positive-ion mode) *m*/*z* 737.3301 $[M + Na]^+$ (calcd. for $C_{42}H_{50}O_{10}Na$, 737.3302).

*Myricone L (**11**):* yellowish gum; $[\alpha]^{20}_D$ +50 (*c* 0.02, MeOH); UV (MeOH) λ_{max} (log ε) 225 (2.91), 272 (2.51), and 340 (1.78) nm; IR (KBr) ν_{max} 2938, 2834, 1631, 1503, 1276, 1030, and 697 cm^{-1}; ECD (MeOH) λ_{max} ($\Delta\varepsilon$) 211 (+38.25), 226 (+8.96), 237 (+4.23), 247 (−1.80), 288 (−4.15) nm; ^{1}H NMR (500 MHz) and ^{13}C NMR (125 MHz) data in chloroform-*d* (Tables S.3 and S.4), in acetone-d_6 (Table S.13); HRESIMS (positive-ion mode) *m*/*z* 737.3303 $[M + Na]^+$ (calcd. for $C_{42}H_{50}O_{10}Na$, 737.3302).

*Myricone M (**12**):* yellowish gum; $[\alpha]^{20}_D$ +26 (*c* 0.04, MeOH); UV (MeOH) λ_{max} (log ε) 227 (2.92), 272 (2.73), and 340 (2.08) nm; IR (KBr) ν_{max} 2933, 2857, 1747, 1592, 1514, 1278, 1056, 1033, and 667 cm^{-1}; ECD (MeOH) λ_{max} ($\Delta\varepsilon$) 225 (−9.82), 244 (−11.95), and 283 (−7.28) nm; ^{1}H NMR (500 MHz) and ^{13}C NMR (125 MHz) data in chloroform-*d* (Tables S.3 and S.4), in acetone-d_6 (Table

https://doi.org/10.1021/acsomega.4c05649
ACS Omega 2024, 9, 35170−35181

S.13); HRESIMS (positive-ion mode) m/z 721.3353 $[M + Na]^+$ (calcd. for $C_{42}H_{50}O_9Na$, 721.3353).

*Myricone N (**13**):* yellowish gum; $[\alpha]^{20}_D$ +33 (c 0.01, MeOH); UV (MeOH) λ_{max} (log ε) 222 (2.63), 272 (1.90), and 340 (1.60) nm; IR (KBr) ν_{max} 2935, 2835, 1683, 1627, 1502, 1227, 1098, 1032, and 674 cm^{-1}; ECD (MeOH) λ_{max} ($\Delta\varepsilon$) 230 (+13.40), 245 (−5.08), and 281 (−3.69) nm; ^1H NMR (500 MHz) and ^{13}C NMR (125 MHz) data in chloroform-*d*, see Tables S.3 and S.4; HRESIMS (positive-ion mode) m/z 721.3353 $[M + Na]^+$ (calcd. for $C_{42}H_{50}O_9Na$, 721.3353).

*Myricone O (**14**):* yellowish gum; $[\alpha]^{20}_D$ +131 (c 0.03, MeOH); UV (MeOH) λ_{max} (log ε) 230 (2.94), 279 (2.82), and 356 (2.08) nm; IR (KBr) ν_{max} 2925, 2855, 1746, 1694, 1513, 1246, 1034, and 667 cm^{-1}; ECD (MeOH) λ_{max} ($\Delta\varepsilon$) 241 (+13.66) nm; ^1H NMR (500 MHz) and ^{13}C NMR (125 MHz) data in chloroform-*d*, see Table 1; HRESIMS (positive-ion mode) m/z 707.3196 $[M + Na]^+$ (calcd. for $C_{41}H_{48}O_9Na$, 707.3196).

*Myricone P (**15**):* yellowish gum; $[\alpha]^{20}_D$ +54 (c 0.02, MeOH); UV (MeOH) λ_{max} (log ε) 223 (2.79), 279 (2.41), and 356 (1.74) nm; IR (KBr) ν_{max} 2935, 1746, 1603, 1513, 1227, 1033, and 667 cm^{-1}; ECD (MeOH) λ_{max} ($\Delta\varepsilon$) 241 (+11.49) nm; ^1H NMR (500 MHz) and ^{13}C NMR (125 MHz) data in chloroform-*d* (Table S.5), in acetone-d_6 (Table S.14); HRESIMS (positive-ion mode) m/z 709.3356 $[M + Na]^+$ (calcd. for $C_{41}H_{50}O_9Na$, 709.3353).

*Myricone R (**16**):* yellowish gum; $[\alpha]^{20}_D$ +41 (c 0.01, MeOH); UV (MeOH) λ_{max} (log ε) 223 (2.86), 279 (2.45), and 359 (1.78) nm; IR (KBr) ν_{max} 2925, 2853, 1602, 1514, 1270, and 1034 cm^{-1}; ECD (MeOH) λ_{max} ($\Delta\varepsilon$) 241 (−16.29) nm; ^1H NMR (500 MHz) and ^{13}C NMR (125 MHz) data in chloroform-*d*, see Table S.5; HRESIMS (positive-ion mode) m/z 709.3353 $[M + Na]^+$ (calcd. for $C_{41}H_{50}O_9Na$, 709.3353).

*Myricone Q (**17**):* yellowish gum; $[\alpha]^{20}_D$ −22 (c 0.01, MeOH); UV (MeOH) λ_{max} (log ε) 227 (2.97), 273 (2.87), and 343 (1.85) nm; IR (KBr) ν_{max} 2924, 2863, 1746, 1601, 1518, 1288, 1053, and 1033 cm^{-1}; ECD (MeOH) λ_{max} ($\Delta\varepsilon$) 241 (+2.20) and 274 (−4.90) nm; ^1H NMR (500 MHz) and ^{13}C NMR (125 MHz) data in chloroform-*d* (Table 1), in acetone-d_6 (Table S.15); HRESIMS (positive-ion mode) m/z 705.3040 $[M + Na]^+$ (calcd. for $C_{41}H_{46}O_9Na$, 705.3040).

*Myricone T (**18**):* yellowish gum; $[\alpha]^{20}_D$ −19 (c 0.01, MeOH); UV (MeOH) λ_{max} (log ε) 230 (1.16), 273 (1.74), and 345 (0.70) nm; IR (KBr) ν_{max} 2947, 2885, 1747, 1641, 1574, 1027, and 659 cm^{-1}; ECD (MeOH) λ_{max} ($\Delta\varepsilon$) 241 (+2.15) and 275 (−3.86) nm; ^1H NMR (500 MHz) and ^{13}C NMR (125 MHz) data in chloroform-*d* (Table S.6), in acetone-d_6 (Table S.15); HRESIMS (positive-ion mode) m/z 705.3042 $[M + Na]^+$ (calcd. for $C_{41}H_{46}O_9Na$, 705.3040).

*Myricone X (**19**):* yellowish gum; $[\alpha]^{20}_D$ −16 (c 0.02, MeOH); UV (MeOH) λ_{max} (log ε) 233 (2.04), 273 (2.16), and 352 (1.18) nm; IR (KBr) ν_{max} 2935, 2853, 1732, 1625, 1502, 1226, 1059, 1028, and 697 cm^{-1}; ECD (MeOH) λ_{max} ($\Delta\varepsilon$) 241 (+3.02) and 275 (−3.71) nm; ^1H NMR (500 MHz) and ^{13}C NMR (125 MHz) data in chloroform-*d* (Table S.6), in acetone-d_6 (Table S.15); HRESIMS (positive-ion mode) m/z 705.3042 $[M + Na]^+$ (calcd. for $C_{41}H_{46}O_9Na$, 705.3040).

*Myricone Y (**20**):* white amorphous powder; $[\alpha]^{20}_D$ −51 (c 0.01, MeOH); UV (MeOH) λ_{max} (log ε) 202 (3.34), 222 (3.18), and 325 (3.16) nm; IR (KBr) ν_{max} 3734, 3645, 2938, 2862, 1746, 1602, 1518, 1269, 1054, 1032, and 655 cm^{-1}; ECD (MeOH) λ_{max} ($\Delta\varepsilon$) 223 (7.10), 244 (6.81), 276 (0.73), and 320 (−9.40) nm; ^1H NMR (500 MHz) and ^{13}C NMR (125 MHz) data in methanol-d_4, see Table S.6; HRESIMS (positive-ion mode) m/z 379.1157 $[M + Na]^+$ (calcd. for $C_{20}H_{20}O_6Na$, 379.1158).

*Myricone Z (**21**):* yellowish gum; UV (MeOH) λ_{max} (log ε) 231 (2.72), 271 (2.45), and 350 (1.54) nm; IR (KBr) ν_{max} 2924, 2860, 1746, 1603, 1513, 1277, 1001, and 666 cm^{-1}; ^1H NMR (500 MHz) and ^{13}C NMR (125 MHz) data in chloroform-*d*, see Table 2; HRESIMS (positive-ion mode) m/z 557.2515 $[M + Na]^+$ (calcd. for $C_{32}H_{38}O_7Na$, 557.2515).

*Myricone W (**22**):* yellowish gum; UV (MeOH) λ_{max} (log ε) 231 (2.95), 270 (2.86), and 340 (1.85) nm; IR (KBr) ν_{max} 2937, 2844, 1746, 1600, 1512, 1226, 1033, and 667 cm^{-1}; ^1H NMR (500 MHz) and ^{13}C NMR (125 MHz) data in chloroform-*d*, see Table S.7; HRESIMS (positive-ion mode) m/z 557.2516 $[M + Na]^+$ (calcd. for $C_{32}H_{38}O_7Na$, 557.2515).

*Myricone J (**41**):* yellowish gum; $[\alpha]^{20}_D$ +36 (c 0.01, MeOH); UV (MeOH) λ_{max} (log ε) 232 (3.01), 274 (2.85), and 338 (2.23) nm; IR (KBr) ν_{max} 2924, 2851, 1693, 1620, 1591, 1515, 1452, 1335, 1279, 1227, 1150, 1126, and 1060 cm^{-1}; ECD (MeOH) λ_{max} ($\Delta\varepsilon$) 227 (−11.28), 244 (−15.19), and 283 (−8.47) nm; ^1H NMR (500 MHz) and ^{13}C NMR (125 MHz) data in chloroform-*d*, see Tables S.3 and S.4; HRESIMS (positive-ion mode) m/z 737.3304 $[M + Na]^+$ (calcd. for $C_{42}H_{50}O_{10}Na$, 737.3302).

*Myricone S (**42**):* yellowish gum; $[\alpha]^{20}_D$ +29 (c 0.02, MeOH); UV (MeOH) λ_{max} (log ε) 215 (2.83), 267 (2.67), and 343 (1.78) nm; IR (KBr) ν_{max} 2923, 2851, 1693, 1628, 1597, 1509, 1453, 1341, 1262, 1236, 1140, 1091, 1060, 1044, and 667 cm^{-1}; ECD (MeOH) λ_{max} ($\Delta\varepsilon$) 214 (−12.33), 222 (+6.86) nm; ^1H NMR (500 MHz) and ^{13}C NMR (125 MHz) data in chloroform-*d*, see Tables S.3 and S.4; HRESIMS (positive-ion mode) m/z 707.3196 $[M + Na]^+$ (calcd. for $C_{41}H_{48}O_9Na$, 707.3196).

*Myricone U (**43**):* yellowish gum; $[\alpha]^{20}_D$ +93 (c 0.03, MeOH); UV (MeOH) λ_{max} (log ε) 240 (3.10), 277 (3.06), and 354 (2.40) nm; IR (KBr) ν_{max} 2922, 2850, 1693, 1602, 1513, 1488, 1432, 1212, 1138, 1039, 1005, and 699 cm^{-1}; ECD (MeOH) λ_{max} ($\Delta\varepsilon$) 241 (+17.60) nm; ^1H NMR (500 MHz) and ^{13}C NMR (125 MHz) data in chloroform-*d*, see Table S.5; HRESIMS (positive-ion mode) m/z 691.3246 $[M + Na]^+$ (calcd. for $C_{41}H_{48}O_8Na$, 691.3247).

*Myfracone A (**44**):* yellowish gum; $[\alpha]^{20}_D$ +17 (c 0.03, MeOH); UV (MeOH) λ_{max} (log ε) 232 (2.60), 274 (2.49), and 354 (1.78) nm; IR (KBr) ν_{max} 2922, 2850, 1692, 1619, 1525, 1436, 1341, 1213, 1140, 1004, 956, and 700 cm^{-1}; ECD (MeOH) λ_{max} ($\Delta\varepsilon$) 217 (+2.91), 234 (−1.37) nm; ^1H NMR (500 MHz) and ^{13}C NMR (125 MHz) data in chloroform-*d*, see Tables S.8 and S.9; HRESIMS (positive-ion mode) m/z 515.2774 $[M + Na]^+$ (calcd. for $C_{31}H_{40}O_5Na$, 515.2773).

*Myfracone B (**45**):* yellowish gum; $[\alpha]^{20}_D$ −29 (c 0.01, MeOH); UV (MeOH) λ_{max} (log ε) 230 (2.11), 270 (2.28), and 290 (1.65) nm; IR (KBr) ν_{max} 2923, 2851, 1692, 1628, 1598, 1508, 1452, 1365, 1291, 1238, 1138, 1094, 1041, and 701 cm^{-1}; ECD (MeOH) λ_{max} ($\Delta\varepsilon$) 211 (−12.78), 230 (−1.92) nm; ^1H NMR (500 MHz) and ^{13}C NMR (125 MHz) data in chloroform-*d*, see Tables S.8 and S.9; HRESIMS (positive-ion mode) m/z 517.2929 $[M + Na]^+$ (calcd. for $C_{31}H_{42}O_5Na$, 517.2930).

*Myfracone C (**46**):* yellowish gum; $[\alpha]^{20}_D$ −15 (c 0.02, MeOH); UV (MeOH) λ_{max} (log ε) 228 (2.48), 278 (2.04), and 352 (1.40) nm; IR (KBr) ν_{max} 2923, 2850, 1693, 1600, 1524, 1429, 1365, 1280, 1239, 1138 cm^{-1}; ECD (MeOH) λ_{max}

https://doi.org/10.1021/acsomega.4c05649
ACS Omega 2024, 9, 35170−35181

($\Delta\varepsilon$) 201 (−23.95), 233 (−2.15) nm; ^{1}H NMR (500 MHz) and ^{13}C NMR (125 MHz) data in chloroform-*d*, see Tables S.8 and S.9; HRESIMS (positive-ion mode) *m*/*z* 517.2930 [M + Na]$^+$ (calcd. for $C_{31}H_{42}O_5Na$, 517.2930).

*Myfracone D (**47**):* yellowish gum; $[\alpha]^{20}_D$ +42 (*c* 0.02, MeOH); UV (MeOH) λ_{max} (log ε) 227 (2.56), 275 (2.23), and 352 (1.57) nm; IR (KBr) ν_{max} 2923, 2851, 1692, 1628, 1598, 1524, 1424, 1363, 1240, 1211, 1138, 1045, 1001, and 808 cm^{-1}; ECD (MeOH) λ_{max} ($\Delta\varepsilon$) 203 (−13.17), 216 (−2.58) nm; ^{1}H NMR (500 MHz) and ^{13}C NMR (125 MHz) data in chloroform-*d*, see Table 2; HRESIMS (positive-ion mode) *m*/*z* 517.2929 [M + Na]$^+$ (calcd. for $C_{31}H_{42}O_5Na$, 517.2930).

*Myfracone E (**48**):* yellowish gum; $[\alpha]^{20}_D$ +28 (*c* 0.03, MeOH); UV (MeOH) λ_{max} (log ε) 227 (2.34), 275 (1.85), and 352 (1.11) nm; IR (KBr) ν_{max} 2923, 2852, 1692, 1599, 1521, 1422, 1363, 1240, 1211, 1137, 1118, 1042, and 807 cm^{-1}; ECD (MeOH) λ_{max} ($\Delta\varepsilon$) 201 (−20.91), 216 (+3.38) nm; ^{1}H NMR (500 MHz) and ^{13}C NMR (125 MHz) data in chloroform-*d*, see Tables S.8 and S.9; HRESIMS (positive-ion mode) *m*/*z* 517.2927 [M + Na]$^+$ (calcd. for $C_{31}H_{42}O_5Na$, 517.2930).

*Myfracone F (**49**):* yellowish gum; $[\alpha]^{20}_D$ +53 (*c* 0.03, MeOH); UV (MeOH) λ_{max} (log ε) 244 (3.22), 272 (3.23), and 292 (3.06) nm; IR (KBr) ν_{max} 2920, 2849, 1692, 1629, 1595, 1508, 1453, 1375, 1272, 1238, 1212, 1138, 1094, 1036, and 700 cm^{-1}; ECD (MeOH) λ_{max} ($\Delta\varepsilon$) 204 (+37.13), 217 (−4.74) nm; ^{1}H NMR (500 MHz) and ^{13}C NMR (125 MHz) data in chloroform-*d*, see Tables S.8 and S.9; HRESIMS (positive-ion mode) *m*/*z* 543.2358 [M + Na]$^+$ (calcd. for $C_{31}H_{36}O_7Na$, 543.2359).

*Myfracone G (**50**):* yellowish gum; $[\alpha]^{20}_D$ −39 (*c* 0.01, MeOH); UV (MeOH) λ_{max} (log ε) 224 (2.49), 272 (2.11), and 350 (1.48) nm; IR (KBr) ν_{max} 2929, 2857, 1604, 1516, 1430, 1370, 1280, 1252, 1212, 1114, 1094, and 722 cm^{-1}; ECD (MeOH) λ_{max} ($\Delta\varepsilon$) 209 (+2.78), 222 (+1.47), 246 (−0.38), 266 (−0.28) nm; ^{1}H NMR (500 MHz) and ^{13}C NMR (125 MHz) data in chloroform-*d*, see Tables S.8 and S.9; HRESIMS (positive-ion mode) *m*/*z* 533.2878 [M + Na]$^+$ (calcd. for $C_{31}H_{42}O_6Na$, 533.2879).

*Myfracone H (**51**):* yellowish gum; $[\alpha]^{20}_D$ −49 (*c* 0.02, MeOH); UV (MeOH) λ_{max} (log ε) 222 (2.70), 278 (2.18), and 338 (1.60) nm; IR (KBr) ν_{max} 2929, 2854, 1604, 1592, 1515, 1452, 1333, 1277, 1233, 1128, 1070, and 721 cm^{-1}; ECD (MeOH) λ_{max} ($\Delta\varepsilon$) 206 (−41.86), 218 (+8.28), 224 (−5.95), 235 (−3.27), 245 (+8.87), 288 (+16.52) nm; ^{1}H NMR (500 MHz) and ^{13}C NMR (125 MHz) data in chloroform-*d* (Tables S.3 and S.4), in acetone-d_6 (Table S.13); HRESIMS (positive-ion mode) *m*/*z* 737.3304 [M + Na]$^+$ (calcd. for $C_{42}H_{50}O_{10}Na$, 737.3302).

*Myfracone I (**52**):* yellowish gum; UV (MeOH) λ_{max} (log ε) 224 (2.45), 268 (2.00), and 352 (0.90) nm; IR (KBr) ν_{max} 2924, 2850, 1628, 1600, 1513, 1452, 1261, 1227, 1138, and 1021 cm^{-1}; ^{1}H NMR (500 MHz) and ^{13}C NMR (125 MHz) data in chloroform-*d*, see Table S.7; HRESIMS (positive-ion mode) *m*/*z* 557.2516 [M + Na]$^+$ (calcd. for $C_{32}H_{38}O_7Na$, 557.2515).

Coupling Constant Simulation. The 3D structures of two possible diastereomers of compounds **1**, **2**, **10**, and **11** and the 10*R**,11*R**- and 10*S**,11*R**-forms were generated and minimized at the MM2 level of theory in Chem3D 19.0. The coupling constants between H-10 and H-11 of the two resulting structures were predicted using Maestro 10.6 (version 2016−2, Schrödinger LLC).

NMR Simulation. MestReNova Version 14.1.2−25024 was used to simulate the H-11 peak of **14**. The "Spin Simulation" under the "Prediction" tab was clicked to open the dialogue box. The "Spin Groups" was set to "4", the "Shifts (ppm)" values of "A" to "D" were "2.26", "4.18", "0.74", and "4.232", respectively, "N" values were set to "1" for "A", "B", and "D" and "3" for "C", and the "Line Width" was set to "5.0". After the coupling constants between H-10, H-11, H-12, and H-14 had been set as 11.9 ($J_{H\text{-}10/H\text{-}11}$), 6.7 ($J_{H\text{-}11/H\text{-}14}$), and 0−12 Hz ($J_{H\text{-}11/H\text{-}12}$), the icon with "New Simulation" at the top left was clicked to generate the simulated ^{1}H NMR peak of H-11.

ECD Calculation. Compounds **1**−**4**, **6**, **10**−**16**, and **44**−**49** were simplified to perform ECD calculation (Figure S.35). The conformers of simplified **1**−**4**, **6**, **10**−**16**, and **44**−**49** used in this research were found using the Macromodel (version 2022-1, Schrödinger LLC) module with "mixed torsional/Low-mode sampling" in the MMFF force field. The searches were conducted in the gas phase, applying a 5 kJ/mol energy window limit and a maximum of 10000 steps to explore all potential conformers. Conformer minimization employed the Polak−Ribiere Conjugate Gradient (PRCG) method with 10000 iterations and a convergence threshold of 0.001 kJ (mol Å)$^{-1}$ on the Root Mean Square (RMS) gradient. Geometry optimization of all conformers was performed using Gaussian 16 software (Gaussian Inc.) in the gas phase at the B3LYP/6-31G(d) level. Subsequently, excitation energies, oscillator strength, and rotatory strength were calculated at the same B3LYP/6-31G(d) level by using the Polarizable Continuum Model (PCM) with methanol as the solvent. The ECD spectra were Boltzmann-averaged based on the calculated Gibbs free energy of each conformer (Table S.17) and visualized with SpecDis software (Version 1.71) with a σ/γ value of 0.15 eV for simplified-**1**/**3**, 0.24 eV for simplified-**2**/**4**, 0.27 eV for simplified-**6**, 0.26 eV for simplified-**10**, 0.16 eV for simplified-**11**, 0.23 eV for simplified-**12**, 0.18 eV for simplified-**13**, 0.24 eV for simplified-**14**/**15**, 0.23 eV for simplified-**16**, 0.29 eV for simplified-**44**, 0.22 eV for simplified-**45**, 0.26 eV for simplified-**46**, 0.24 eV for simplified-**47**, 0.28 eV for simplified-**48**, and 0.16 eV for simplified-**49**. Additionally, a UV-shift correction was applied.

Cell Culture. RAW-dual cells (InvivoGen) were grown in 10 cm culture dishes using Dulbecco's modified Eagle's medium (DMEM; HyClone) supplemented with 10% fetal bovine serum (FBS) plus 100 U/mL penicillin/streptomycin (HyClone) and 0.2% Normocin (InvivoGen). RAW 264.7 cells (Korean Cell Line Bank) were cultured in DMEM containing 10% FBS and 100 U/mL penicillin/streptomycin. Cultures were maintained at 37 °C in a humidified atmosphere containing 5% CO_2.

Cell Viability. RAW 264.7 cells were plated at a density of 1.0×10^5 cells per well in 96-well plates and incubated for 24 h. Cell viability was assessed by adding 3-(4,5-dimethylthiazol-2-yl)-2,5-diphenyltetrazolium bromide (MTT) solution to the cells (final concentration: 0.5 mg/mL) and incubating for 1 h at 37 °C. The absorbance of the solubilized formazan product was measured using a spectrophotometer (BioTek Instruments).

Quantification of NF-κB/AP-1 and IRF Activity. RAW-Dual cells were seeded at 1×10^5 cells/well in a 96-well plate. RAW-Dual cells secreted embryonic alkaline phosphatase (SEAP), and Luciferase reporter cells were pretreated with

https://doi.org/10.1021/acsomega.4c05649
ACS Omega 2024, 9, 35170−35181

12.5, 25, 50 μg/mL compounds for 1 h and then stimulated with TLR agonist for 18 h. The supernatants were recovered. SEAP activity was measured by QUANTI-Blue assay (InvivoGen) and Luciferase activity was measured by QUANTI-Luc assay (InvivoGen).

Enzyme-Linked Immunosorbent Assay (ELISA) and Nitric Oxide (NO) Assay. RAW 264.7 cells were seeded at 1×10^5 cells/well in a 96-well plate. After 24 h of secretion of interleukin (IL)-6, the culture supernatants from the cells were analyzed using LEGEND MAX mouse IL-6 ELISA kits (BioLegned). The secretion of NO was measured by using the Griess reagent (Sigma). The optical density of the solubilized formazan product was measured by using a spectrophotometer.

Statistical Analysis. Statistical analysis was performed with GraphPad Prism, version 7.0 (GraphPad, San Diego, CA, USA). An unpaired two-tailed *t* test with a 95% confidence interval was used for the calculation of the *p* values. Group sizes, reproducibility, and *p* values for each experiment are given in the figure legends.

■ ASSOCIATED CONTENT

Supporting Information

. The Supporting Information is available free of charge at https://pubs.acs.org/doi/10.1021/acsomega.4c05649.

1D, 2D NMR, and HR-ESI-MS spectra for all new compounds, structural determination of remaining new compounds, and experimental and calculated ECD spectra of compounds (PDF)

■ AUTHOR INFORMATION

Corresponding Authors

Chung Sub Kim − *Department of Biopharmaceutical Convergence and School of Pharmacy, Sungkyunkwan University, Suwon 16419, Republic of Korea;* orcid.org/0000-0001-9961-4093; Email: chungsub.kim@skku.edu

Sang Hoon Jung − *Natural Product Research Center, Korea Institute of Science and Technology (KIST), Gangneung 25451, Republic of Korea; Division of Bio-Medical Science & Technology, KIST School, University of Science and Technology, Gangneung 25451, Republic of Korea;* orcid.org/0000-0003-1009-0727; Email: shjung507@gmail.com

Authors

Tam Thi Le − *Natural Product Research Center, Korea Institute of Science and Technology (KIST), Gangneung 25451, Republic of Korea*

Jonghwan Kim − *Department of Biopharmaceutical Convergence, Sungkyunkwan University, Suwon 16419, Republic of Korea*

Tae Kyeom Kang − *Natural Product Research Center, Korea Institute of Science and Technology (KIST), Gangneung 25451, Republic of Korea*

Wook-Bin Lee − *Natural Product Research Center, Korea Institute of Science and Technology (KIST), Gangneung 25451, Republic of Korea*

Myungsuk Kim − *Natural Product Research Center, Korea Institute of Science and Technology (KIST), Gangneung 25451, Republic of Korea; Division of Bio-Medical Science & Technology, KIST School, University of Science and Technology, Gangneung 25451, Republic of Korea*

Complete contact information is available at: https://pubs.acs.org/10.1021/acsomega.4c05649

Author Contributions

T.T.L. and J.K. contributed equally to this work. T.T.L.: methodology, formal analysis, data curation, writing−review and editing. J.K.: methodology, formal analysis, data curation, writing. T.K.K.: methodology, formal analysis, writing. W.-B.L.: writing−review and editing. M.K.: resources, funding acquisition, writing−review and editing. C.S.K.: supervision, writing−review and editing. S.H.J.: supervision, funding acquisition, conceptualization, methodology, formal analysis, visualization, writing−review and editing.

Funding

This work was supported by the Korea Institute of Science and Technology Intramural Research Grants (2E32621).

Notes

The authors declare no competing financial interest.

■ ACKNOWLEDGMENTS

We are thankful to the Korea Basic Science Institute (KBSI) for the mass spectrometric measurements.

■ REFERENCES

(1) Periasamy, G. K. A.; Gibrelibanos, M.; Gebremedhin, G. Nutmeg (Myristica fragrans Houtt.) oils. In *Essential oils in food preservation, favor and safety*; Preedy, V. R., Ed.; Elsevier: 2016; pp 607−616

(2) Adjene, J. O.; Igbigbi, P. S. Effect of chronic consumption of nutmeg on the stomach of adult wistar rats. *Fooyin Journal of Health Sciences* **2010**, *2* (3), 62−65.

(3) Hattori, M.; Yang, X. W.; Shu, Y. Z.; Kakiuchi, N.; Tezuka, Y.; Kikuchi, T.; Namba, T. New constituents of the aril of *Myristica fragrans*. *Chem. Pharm. Bull.* **1988**, *36* (2), 648−653.

(4) Hattori, M.; Yang, X. W.; Miyashiro, H.; Namba, T. Inhibitory effects of monomeric and dimeric phenylpropanoids from mace on lipid peroxidation *in-vivo* and *in-vitro*. *Phytotherapy Research* **1993**, *7* (6), 395−401.

(5) Ha, M. T.; Vu, N. K.; Tran, T. H.; Kim, J. A.; Woo, M. H.; Min, B. S. Phytochemical and pharmacological properties of *Myristica fragrans* Houtt.: an updated review. *Archives of Pharmacal Research* **2020**, *43* (11), 1067−1092.

(6) Li, F.; Yang, X. W. Three new neolignans from the aril of *Myristica fragrans*. *Helv. Chim. Acta* **2007**, *90* (8), 1491−1496.

(7) Duan, L.; Tao, H. W.; Hao, X. J.; Gu, Q. Q.; Zhu, W. M. Cytotoxic and antioxidative phenolic compounds from the traditional chinese medicinal plant. *Myristica fragrans*. *Planta Medica* **2009**, *75* (11), 1241−1245.

(8) Kapoor, I. P. S.; Singh, B.; Singh, G.; De Heluani, C. S.; De Lampasona, M. P.; Catalan, C. A. N. Chemical composition and antioxidant activity of essential oil and oleoresins of nutmeg (*Myristica fragrans* Houtt.) fruits. *International Journal of Food Properties* **2013**, *16* (5), 1059−1070.

(9) Hou, J. P.; Wu, H.; Wang, Y.; Weng, X. C. Isolation of some compounds from nutmeg and their antioxidant activities. *Czech Journal of Food Sciences* **2012**, *30* (2), 164−170.

(10) Olajide, O. A.; Makinde, J. M.; Awe, S. O. Evaluation of the pharmacological properties of nutmeg oil in rats and mice. *Pharmaceutical Biology* **2000**, *38* (5), 385−390.

(11) Munoz Acuna, U.; Carcache, P. J. B.; Matthew, S.; Carcache de Blanco, E. J. New acyclic bis phenylpropanoid and neolignans, from *Myristica fragrans* Houtt., exhibiting PARP-1 and NF-κB inhibitory effects. *Food Chem.* **2016**, *202*, 269−275.

(12) Orabi, K. Y.; Mossa, J. S.; el-Feraly, F. S. Isolation and characterization of two antimicrobial agents from mace (*Myristica fragrans*). *J. Nat. Prod.* **1991**, *54* (3), 856−859.

(13) Park, S.; Lee, D. K.; Yang, C. H. Inhibition of fos-jun-DNA complex formation by dihydroguaiaretic acid and in vitro cytotoxic effects on cancer cells. *Cancer Letters* **1998**, *127* (1−2), 23−28.
(14) Lee, J. Y.; Park, W. Anti-inflammatory effect of myristicin on RAW 264.7 macrophages stimulated with polyinosinic-polycytidylic acid. *Molecules* **2011**, *16* (8), 7132−7142.
(15) Cao, G. Y.; Xu, W.; Yang, X. W.; Gonzalez, F. J.; Li, F. New neolignans from the seeds of *Myristica fragrans* that inhibit nitric oxide production. *Food Chem.* **2015**, *173*, 231−237.
(16) Tsukayama, I.; Kawakami, Y.; Tamenobu, A.; Toda, K.; Maruoka, S.; Nagasaki, Y.; Mori, Y.; Sawazumi, R.; Okamoto, K.; Kanzaki, K.; Ito, H.; Takahashi, Y.; Miki, Y.; Yamamoto, K.; Murakami, M.; Suzuki-Yamamoto, T. Malabaricone C derived from nutmeg inhibits arachidonate 5-lipoxygenase activity and ameliorates psoriasis-like skin inflammation in mice. *Free Radical Biol. Med.* **2022**, *193*, 1−8.
(17) Ma, J. H.; Hwang, Y. K.; Cho, W. H.; Han, S. H.; Hwang, J. K.; Han, J. S. Macelignan attenuates activations of mitogen-activated protein kinases and nuclear factor kappa B induced by lipopolysaccharide in microglial cells. *Biol. Pharm. Bull.* **2009**, *32* (6), 1085−1090.
(18) Jin, H.; Zhu, Z. G.; Yu, P. J.; Wang, G. F.; Zhang, J. Y.; Li, J. R.; Ai, R. T.; Li, Z. H.; Tian, Y. X.; Xu, W.; Zhang, J. J.; Wu, S. G. Myrislignan attenuates lipopolysaccharide-induced inflammation reaction in murine macrophage cells through inhibition of NF-κB signalling pathway activation. *Phytotherapy Research* **2012**, *26* (9), 1320−1326.
(19) Oanh, V. T.; Phong, N. V.; Min, B. S.; Yang, S. Y.; Kim, J. A. Insights into the inhibitory activities of neolignans and diarylnonanoid derivatives from nutmeg (*Myristica fragrans* Houtt.) seeds on soluble epoxide hydrolase using and approaches. *Journal of Enzyme Inhibition and Medicinal Chemistry* **2023**, *38* (1), 2251099.
(20) Greca, M. D.; Molinaro, A.; Monaco, P.; Previtera, L. Neolignans from *Arum italicum*. *Phytochemistry* **1994**, *35* (3), 777−779.
(21) Gellerstedt, G.; Lundquist, K.; Wallis, A. F. A.; Zhang, L. M. Revised structures for neolignans from *Arum italicum*. *Phytochemistry* **1995**, *40* (1), 263−265.
(22) Huo, C. H.; Liang, H.; Zhao, Y. Y.; Wang, B.; Zhang, Q. Y. Neolignan glycosides from *Symplocos caudata*. *Phytochemistry* **2008**, *69* (3), 788−795.
(23) Herrera Braga, A. C.; Zacchino, S.; Badano, H.; Sierra, M. G.; Ruveda, E. A. ^{13}C NMR spectral and conformational analysis of 8-O-4' neolignans. *Phytochemistry* **1984**, *23* (9), 2025−2028.
(24) Nakatani, N.; Ikeda, K.; Kikuzaki, H.; Kido, M.; Yamaguchi, Y. Diaryldimethylbutane lignans from myristica argentea and their antimicrobial action against *Streptococcus* Mutans. *Phytochemistry* **1988**, *27* (10), 3127−3129.
(25) Silva, D. H. S.; Davino, S. C.; Barros, S. B. D.; Yoshida, M. Dihydrochalcones and flavonolignans from *Iryanthera lancifolia*. *J. Nat. Prod.* **1999**, *62* (11), 1475−1478.
(26) Enriquez, R. G.; Chavez, M. A.; Reynolds, W. F. Phytochemical investigations of plants of the genus *Aristolochia*, 1. Isolation and NMR spectral characterization of eupomatenoid derivatives. *J. Nat. Prod.* **1984**, *47* (5), 896−899.
(27) Cao, G. Y.; Yang, X. W.; Xu, W.; Li, F. New inhibitors of nitric oxide production from the seeds of *Myristica fragrans*. *Food Chem. Toxicol.* **2013**, *62*, 167−171.
(28) Morikawa, T.; Hachiman, I.; Matsuo, K.; Nishida, E.; Ninomiya, K.; Hayakawa, T.; Yoshie, O.; Muraoka, O.; Nakayama, T. Neolignans from the arils of *Myristica fragrans* as potent antagonists of CC chemokine receptor 3. *J. Nat. Prod.* **2016**, *79* (8), 2005−2013.
(29) Du, S. S.; Yang, K.; Wang, C. F.; You, C. X.; Geng, Z. F.; Guo, S. S.; Deng, Z. W.; Liu, Z. L. Chemical constituents and activities of the essential oil from *Myristica fragrans* against cigarette beetle lasioderma serricorne. *Chemistry & Biodiversity* **2014**, *11* (9), 1449−1456.
(30) Niculau, E. D.; Ribeiro, L. D.; Ansante, T. F.; Fernandes, J. B.; Forim, M. R.; Vieira, P. C.; Vendramim, J. D.; da Silva, M. F. D. F. Isolation of chavibetol and methyleugenol from essential oil of *Pimenta pseudocaryophyllus* by high performance liquid chromatography. *Molecules* **2018**, *23* (11), 2909.
(31) Niyas, Z.; Variyar, P. S.; Gholap, A. S.; Sharma, A. Effect of gamma-irradiation on the lipid profile of nutmeg (*Myristica fragrans* Houtt.). *J. Agric. Food Chem.* **2003**, *51* (22), 6502−6504.
(32) Kuo, P. C.; Chen, G. F.; Yang, M. L.; Lin, Y. H.; Peng, C. C. Chemical constituents from the fruits of *Forsythia suspensa* and their antimicrobial activity. *Biomed Research International* **2014**, *2014*, 304830.
(33) Nishida, R.; Shelly, T. E.; Kaneshiro, K. Y. Acquisition of female attracting fragrance by males of Oriental fruit fly from a Hawaiian lei flower. *Fagraea berteriana*. *Journal of Chemical Ecology* **1997**, *23* (10), 2275−2285.
(34) Elferaly, F. S.; Hoffstetter, M. D. Isolation, characterization and synthesis of 3-methoxy-4,5-methylenedioxycinnamaldehyde: A novel constituent from *Canella winterana*. *J. Nat. Prod.* **1980**, *43* (3), 407−410.
(35) Pham, V. C.; Jossang, A.; Sévenet, T.; Bodo, B. Novel cytotoxic acylphenol dimers of *Myristica gigantea*; enzymatic synthesis of giganteones A and B. *Tetrahedron* **2002**, *58* (28), 5709−5714.
(36) Maia, A.; Schmitz-Afonso, I.; Martin, M. T.; Awang, K.; Laprévote, O.; Guéritte, F.; Litaudon, M. Acylphenols from *Myristica crassa* as new acetylcholinesterase inhibitors. *Planta Medica* **2008**, *74* (12), 1457−1462.
(37) Pham, V. C.; Jossang, A.; Sévenet, T.; Bodo, B. Cytotoxic acylphenols from *Myristica maingayi*. *Tetrahedron* **2000**, *56* (12), 1707−1713.
(38) Shen, R. S.; Cao, D.; Chen, F. L.; Wu, X. J.; Gao, J.; Bai, L. P.; Zhang, W.; Jiang, Z. H.; Zhu, G. Y. New monoterpene-conjugated phenolic constituents from nutmeg and their autophagy modulating activities. *J. Agric. Food Chem.* **2022**, *70* (31), 9684−9693.
(39) Gonzalez, M. J. T. G.; Pinto, M. M. M.; Kijjoa, A.; Anantachoke, C.; Herz, W. Stilbenes and other constituents of *Knema austrosiamensis*. *Phytochemistry* **1993**, *32* (2), 433−438.
(40) Forrest, T. P.; Ray, S. 3,4-dimethoxy-trans-cinnamic acid from *Nuphar variegatum*. *Phytochemistry* **1972**, *11* (2), 855.

https://doi.org/10.1021/acsomega.4c05649
ACS Omega 2024, 9, 35170−35181